Journal of Engineering, Science, and Technology
ISSN: 2714-2396 | Volume 6, Issue 2

DEVELOPMENT AND CHARACTERIZATION OF ZEOLITE Y FROM BAMBU CLAY FOR CRACKING OF BIO-OIL

Abdullahi, M. A[1], Garba, M. U[2], Eterigho E. J[2], Alhassan, M[2],
[1,2]Chemical Engineering Department, Federal University of Technology,
PMB 65 Minna, Niger State, Nigeria.
[1]National Agency for Science and Engineering Infrastructure (NASENI), PMB 391 Idu, Garki, Abuja. Federal Capital Territory.
Corresponding author email: abdulmusavespa@gmail.com, +2348035312720

ABSTRACT
Zeolite Y was developed from Bambu clay using two steps of preparation: seed gel and feed gel methods for production of the zeolite. Bambu clay was used as a source of aluminium hydroxide and sodium silicate after undergoing splitting techniques. The clay, meta-kaolin, Synthesis Zeolite Y (SZY), and Commercial Zeolite Y (CZY) were characterised using X-ray Fluorescence (XRF), X-ray diffraction (XRD), Brunauer-Emmett-Teller (BET), Scanning Electron Microscope (SEM), and Fourier Transform Infrared (FTIR) spectroscopy. The acidity of the zeolite Y developed was determined using the pyridine probe acidity test. In order to ascertain that the developed zeolite is Y-type, the results of the SZY were compared with the results of the CZY. The characterization results showed that Bambu clay could be kaolinite clay with a Si/Al ratio of approximately 1:8, and the XRD shows the clay contains kaolinite. The XRF and XRD were complimented using the SEM, which shows that the clay possesses psedo-hexagonal and stacking shapes, which represent a kaolinite structure. The clay possesses Lewis and Bronsted acid sites, which would be a potential source for zeolite synthesis. The analysis shows that the SZY was 2:40, and CZY was 2:46. From the micrograph, the individual particles of SZY and CZY have regular and bulky shapes with average crystallite sizes of 24.77 nm and 24.04 nm, respectively. The BET analysis revealed that the surface area of SZY was 549.10 m2g-1, while that of CZY was 426.20 m2g-1. The acidity analysis showed that the SZY has a higher Lewis site of 220.18 µmol/g than the Bronsted site of 93.44 µmol/g therefore, the SZY is a Lewis acidity type. It can, therefore, be concluded that the characterisation results indicated that SZY has comparatively similar results to CZY in terms of Si/Al ratio, shape, crystallites, crystal structure and possesses milder acidic sites of which could be used for bio-oil cracking.

Keywords: Bambu clay, Zeolite Y, Commercial zeolite Y, Characterization, Bio-oil

1.0 Introduction
The early development of zeolites was carried out by the crystallisation of sodium alumino-silicate gels prepared from pure sodium aluminate, sodium silicate, and sodium hydroxide solutions (Breck, 1974). However, the high cost and limited availability associated with these chemicals have prompted researchers to seek alternative, low-cost raw materials. Some of the unconventional alternative feed stocks are coal fly ash, rice husks, natural clay minerals, and bagasse, among others (Moises et al., 2013). Zeolites are crystalline aluminosilicate minerals with distinctive three-dimensional structural shapes that form uniformly sized interconnected pores of molecular dimensions that are widely used in industrial applications (Asmaa et al., 2020). Natural zeolites possess some drawbacks, including the presence of impurities, inconsistent pore size, and low cation exchange capacity, which favour them for catalytic applications, while synthetic zeolites possess a high active surface area, such as purity and uniformity in particle size and pore size, which favour them for catalytic applications. This is because a larger active surface area allows

more catalytic sites to be exposed, increasing the number of active sites available for reactants to interact with and participate in the catalytic process. (Kwakye-awuah et al., 2014).
Many Researchers developed zeolite Y from locally sourced clay in Nigeria (Salahudee et al., 2018; Ayedoji et al., 2018). Table 1 provides, amongst other things, an overview of Zeolites Y, which are developed from kaolinite clay of various origins in Nigeria. As per our literature survey in this study, the synthesis of Zeolite Y from Bambu clay has not been reported. Therefore, the aim of the study was to develop zeolite Y from Bambu clay, mined from clay deposits in Wamba Local Government Area in Nasarawa State, north-central Nigeria. The clay was used as a source of silica and alumina by the hydrothermal method to produce zeolite Y. The synthesised zeolite Y was further subjected to post-synthetic treatment by heating at high temperatures between 500 ^{0}C – 650 ^{0}C using a furnace so as to remove the remaining water and other molecules present in the zeolite structure for catalytic application.

Table 1.0 An overview of Zeolite Y development from kaolinite clay of various origins in Nigeria.

Source	Treatment method	Si/Al ratio		Pore size (nm)	Bc/Lc ratio	Reference
		Y	ZY			
Kankara Kaolin	Calcination 750^{0}C, 2 h; dealumination H_2SO_4, ambient; gel formation, 100^{0}C, 7 h; drying 110 ^{0}C, 6 h; calcination, 500^{0}C.	Not reported			Very low 0.24	Salahudee et al., 2017
Ado-0do Ota	Metakaolinization at 850^{0}C, 6h; dealumination H_2SO_4, gel 100^{0}C, 7 h; crystallization 100 ^{0}C, 24h.	.46	.22	1.426	Not reporter	Adeoye et al., 2017
Elefun	Calcination 850^{0}C 6h; dealumination H_2SO_4, crystallization 95^{0}C.	.5			Not reported	Ayedoji et al., 2018
Aloji	Calcination 650 ^{0}C for 3 hours, desilication NaoH. Crystallization 80^{0}C, dried 110 ^{0}C 8h	1.12		5.0676	Not reported	Usman et al., 2022

2.0 MATERIALS AND METHOD

2.1 Materials

Bambu clay was collected from clay deposits in Wamba Local Government Area (LGA) (8^0 9600890 N', 8^0 6293780 E') in Nasarawa State, North Central Nigeria. Concentrated sulphuric acid (Sigma-Aldrich, Lobal Chemic, 98%) and Sodium hydroxide pellets (Sigma-Aldrich, Lobal Chemic, ≥ 98%) were used for the development of zeolite Y. The Commercial Zeolite Y used in this study for comparison in terms of Si/Al ratio, surface area, porosity, acidity, and crystal structure were obtained from Kaduna Refinery and Petrochemical Company (KRPC).

2.2 Methods

2.2.1 Preliminary treatment of Bambu clay

A Bambu clay sample was collected from the clay deposits in Wamba Local Government Area (LGA) at a depth interval of 1.0 - 1.5 m with the aid of a shovel and digger. The sample was sorted out by hand to minimize the possibility of contamination with sand. About 50 kg of the sample were collected for the study and placed in polythene bags. For this study, a sub-sample of 10kg was subjected to a preliminary treatment involving the removal of all the dirt associated with clay and sun-dried for one week to ensure the water in the clay had completely evaporated. The dried clay was further ground into smaller particles for characterization to determine its suitability as a precursor for the development of zeolite Y. The clay was beneficiated by sedimentation techniques to produce clay free from impurities.

2.2.2 Beneficiation of bambu clay

The beneficiation was conducted at a clay-to-water ratio of 100 g/litre with an optimum settling time of 24 hours, followed by vigorous stirring at 200 rpm for 3 hours. The slurries were further allowed to settle overnight. The settling of the slurries followed the Stokes law Equation (Patel, 2014) as presented in equation 1.0.

$$r^2 = \frac{9\,\eta h}{2(\rho_1 - \rho_2)gt} \qquad (1.0)$$

2.2.3 Synthesis of zeolite Y

The beneficiated clay was metakaolinised at 750 ^{0}C for 8 hours. The metakaolin was dealuminated by using concentrated sulphuric acid. The splitting of alum and silica method was used in this study; sodium hydroxide was reacted with alum in a ratio of 2.5:1; aluminium hydroxide and sodium silicate were produced from the method. The zeolite was prepared in two steps; Seed gel and feed gel. The seed gel was prepared and allowed to age, while the feed gel was prepared and used immediately without ageing. Locally sourced aluminium hydroxide and sodium silicate from Bambu clay were mixed with sodium hydroxide and deionized water in different proportions. The overall gel was aged at room temperature for 24 hours thereafter, and mole species balance was used to determine the molar composition of the overall gel as $15Na_2O{:}Al_2O_3{:}12SiO_2{:}173H_2O$. The overall aged gel was crystallized at an optimum temperature of 100 ^{0}C for 24 and 48 h. The crystallized mixture of the gel was washed to remove unreacted precursors or soluble by-products and control the pH that was associated with zeolite during gel formulation. Thereafter, it was dried at a moderate temperature of 60 ^{0}C to avoid damage to the zeolite structure. The dried temperature was also supported by Khatrin et al., (2020).

2.2.5 Characterization

To study the Bambu clay, NaY, and HY's crystal structure and relative crystallinity, X-ray diffraction (XRD) was used on an X-ray diffraction machine; the scanning electron micrograph (SEM) was used to know the morphology; and X-ray Fluorescence (XRF) was used to determine chemical composition and mineralogy. Brunauer-Emmett-Teller (BET) analysis was conducted to measure the surface area; Fourier Transform Infrared Spectroscopy (FTIR) was used in the identification of various forms of surface functional groups in the clay; and Pyridine Adsorption for Fourier Transform Infrared Spectroscopy (Py-FTIR) was used to identify the acidity. The characterization was vital for confirming the quality of the synthesis zeolite.

3.0 RESULTS AND DISCUSSION

3.1 X-ray Fluorescence (XRF) analysis

The chemical compositions of Bambu clay, zeolite Y, and commercial zeolite Y obtained from XRF analysis are presented in Table 2. The analysis revealed that Bambu clay can be classified as kaolinite with a Si/Al ratio of 1.8, which implies that the clay could be a potential source for the

production of zeolite Y (Cadene, et al., 2005). The Table shows that the developed zeolite (NaY) is rich in silica and alumina as the main elements, with others in low proportions and traces of elements as contained in the precursor. The Si/Al ratio of the developed NaY is approximately 2.4. Hence, the result obtained was in line with the chemical composition of Y-type zeolites as reported by Asmaa et al. (2020), and the reaction describing the synthesis of zeolite-Y type is given in Equation (1). Also, the Si/Al ratio of the developed zeolite Y is closely similar to the Si/Al ratio of the commercial zeolite Y of 2.62, as presented in Table 2.

$$2NaOH + 2Al(OH)_3 + 2Na_2Si_2O_5 \longrightarrow 2Na_2O + Al_2O_3 + 2Si_2O_5 + 8H_2O \quad (1)$$

Table 2 X-ray Fluorescence (XRF) of the sample

Compound	Raw clay (bambu)	Zeolite Y (NaY)	Commercial Zeolite Y
SiO_2	54.40	50.157	58.157
Al_2O_3	29.30	20.910	22.910
Fe_2O_3	4.20	1.4590	1.4590
CaO	0.41	0.0131	0.0131
V_2O_5	0.029	0.0248	0.0248
K_2O	1.76	0.0305	0.0305
MnO	0.081	0.0040	0.0040
NaO_2	0.80	14.2203	2.1310
TiO_2	1.64	0.8527	0.8527
P_2O_5	ND	Nd	0.5374
SO_3	ND	Nd	0.2182
CuO	0.028	0.0025	0.0025
MgO	0.007	2.6020	2.1600
NiO	-	Nd	0.0071
CuO	0.019	0.0123	0.0123
ZnO	0.012	0.0128	0.0128
Ga_2O_3	-	0.0085	0.0085
PbO	-	-	-
Ta_2O_5	-	0.0029	0.0029
Cl	-	0.7670	1.7670
LOI(1000^0C)			
Si/Al ratio	**1.8**	**2.40**	**2.62**

3.2 X-ray diffraction (XRD) analysis

Figure 1.0 (a-d) presents the X-ray diffractograms of Bambu clay with different peaks, miller indices, and lattice parameters at different diffraction angles and intensities. In Figure 1 (a), the first peaks at 2θ = 8.930 indicated the presence of illite, though the intensity of the peak is not strong enough to justify the presence of illite in appreciable quantity. The second mineral peak at 2θ = 12.500 indicated the presence of kaolinite, the third mineral peak at 2θ = 25.10 indicated the presence of albite, and the fourth mineral peak at 2θ = 26.79 indicated the presence of quartz, which was the highest intensity on the diffraction pattern of bambu clay. Figure 1 (b) shows the XRD pattern of metakaolinized Bambu clay, which contains quartz as the most dominant peak in the Figure. It reveals that kaolinite, illite, and albite minerals were suppressed as a result of calcination, which led their crystal lattice to collapse and their peaks to appear very small in a crisscross pattern. Hence, metakaolin is more reactive than other minerals (Abdullahi et al., 2019).

Figure 1 (c-d) presents the XRD of SZY-type and CZY. The pattern of diffraction peaks of both SZY and CZY has almost the same position of peaks, indices, and lattice constant. These patterns' peak positions, as presented, corroborate the XRD results of Asmaa et al. (2020) and Adeoye et al. (2017).

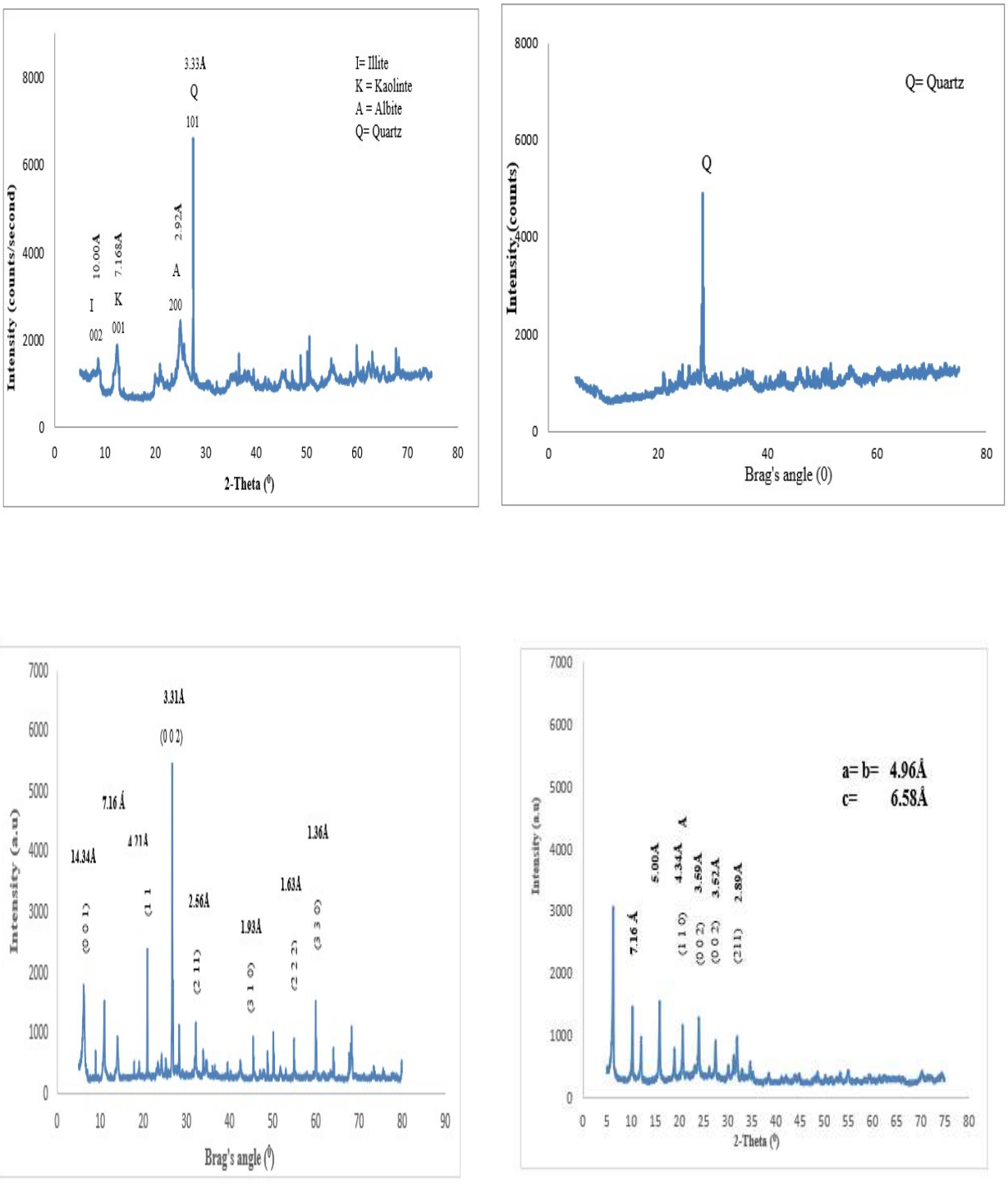

Figure (1) XRD patterns (a) bambu clay, (b) metakaolin (c) SZY (d) CZY

3.3 Scanning Electron Microscopy (SEM)

The morphology and crystallite size of bambu clay, metakaolin, NaY, and CZY were studied as a complementary characterisation technique to the XRD using Scanning Electron Microscopy (SEM) and are presented in Figure 2(a–d). The morphology in Figure 2(a) shows that Bambu clay contains large stacks of highly packed kaolinite (Asmaa et al., 2020). The pseudohexagonal shape is also

present within the microstructure of the clay, which is a characteristic of kaolinite minerals. Figure 2(b) shows that the collapse of other minerals resulted in the appearance of more platy plates lumped together, which indicated the presence of crystalline silica contained in the clay and is evidence of amorphous materials. The SEM image of SZY in Figure 2(c) shows that the individual particles have regular tetrahedral and bulky shapes (Ajayi, 2012), though the shape does not corroborate with the shape explained by Asmaa et al. (2020). Similarly, the CZY shows comparable shapes with the SZY, as presented in Figure (d). The average crystallite size was calculated using Scherer's Equation. The Bambu clay exhibits a crystallite size of 43.55nm; after undergoing metakaolinization, the crystallite size reduces to 29.40nm. The SZY exhibits a comparable crystallite size of 24.77nm with the CZY, which has a crystallite size of 24.04nm and a hexagonal shape. Therefore, based on the classification of pore sizes according to the International Union of Pure and Applied Chemistry (IUPAC) definition, mesopores are between 2 nm and 25 nm hence, Bambu clay, metakaolin, SZY, and CZY are mesoporous based on the estimation of crystallite sizes.

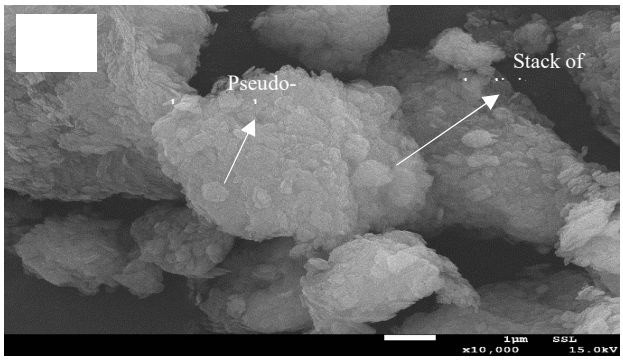

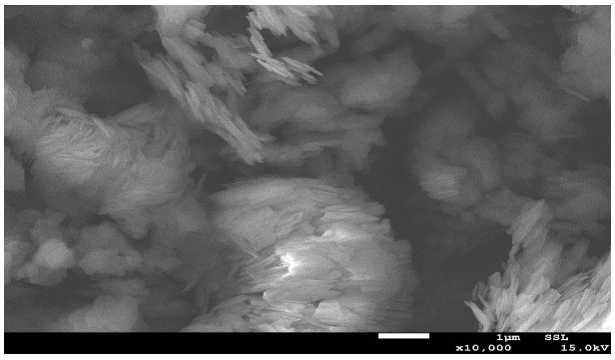

Figure (2): SEM (a) Bambu clay (b) Metakaolin

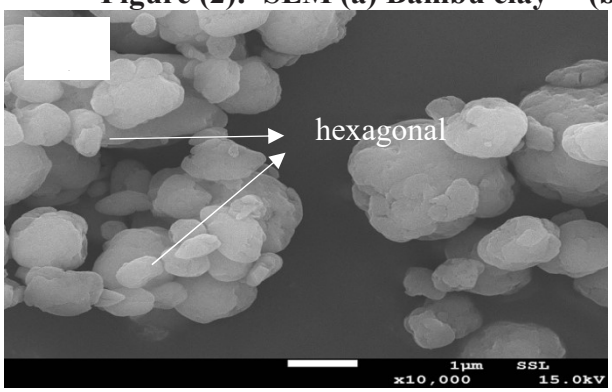

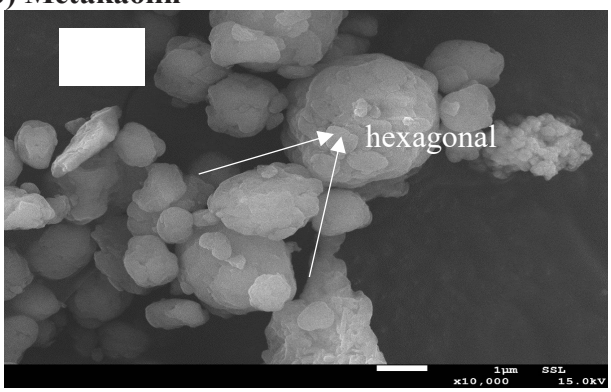

Figure (2): SEM (c) SZY (d) CZY

3.4 Brunauer-Emmett-Teller (BET) analysis of Bamboo clay

6

The BJH method was considered in this research for BET analysis. The BET analysis of the samples reveals that the surface area of Bambu clay was 159.40 m-2g-1. This surface area was higher than the surface area of 45.62 m-2g-1 as revealed by the research work of Ayedoji et al., (2018). This higher surface area of the Bambu clay could enhance the crystallization of zeolite, leading to a more uniform and well-defined product with improved catalytic application. The surface area of SZY was 530.40 m2g-1 which falls within the IUPAC typical ranges of absorbents (zeolites 400 – 900 m2g-1). The surface areas of the samples as presented in Table 3 increase in the following order: Bambu clay<metakaolin<SZY correspond to 150.40 m2g-1<530.40 m2g-1<549.10 m2g-1 respectively. Interestingly, the surface area of SZY is higher than that of CZY, as presented in Table 3. These surface areas are indications of the surface available for reactions. This is because the surface areas as presented could provide a lot of accessibility for the reactants in a limited time to diffuse much more and meet more catalytic sites than smaller surface areas, which could have low diffusion rates. The pore radius of SZY is 3.252nm, a little higher than CZY 3.091 nm; hence, SZY is a mesopore based on the classification of pores according to the IUPAC definition (mesopores 2nm-25nm).

Table 3: BET Results of the porous materials

Samples	BET surface Area m^2g^{-1}	Pore Volume cm^3g^{-1}	Pore Radius (nm)
Raw Bambu clay	159.40	0.078	2.920
Metakaolin	530.40	0.270	3.217
Synthesized zeolite Y	549.10	0.218	3.252
Commercial zeolite Y	426.20	0.214	3.091
Raw clay (Ayedoji et al., 2018)	45.62	0.201	1.79
Synthesis zeolite Y (Khatrin et al., 2020)	451.9	0.2591	1.907

3.5 Acidity analysis of the samples

Table 3 presents the results of the acidity analysis of Bambu clay, metakaolin, SZY and CZY. The analysis shows that the clay contains low Lewis and Bronsted acidic sites of 34.40 and 31.57 µmol/g. This implies that the Bambu clay contains a low acidic site as compared with the results from the research work of Jia et al., (2013) and Nurradeen (2015). The Table shows that the SZY possess Lewis and Bronsted acid sites of 220.18 and 93.44 µmol/g. This implies that the SZY has relatively high values of Lewis acidity and a low Bronsted acidity site, with a very low ratio of Bronsted/Lewis acidity as presented in the Table. Consequently, the SZY is a milder acidic zeolite of the Y-type. It was demonstrated in the research of Maddulur et al., (2019) that milder acidic sites favour catalytic cracking of oxygenated hydrocarbons by selecting the organics in the bio-oil over strong acidic sites.

Table (3) Acidity analysis of the various samples

Samples	Lewis bond (cm^{-1})	Lc Area (µmol)	Bronsted bond (cm^{-1})	Bc Area (µmol)	Lc (µmol/g)	Bc (µmol/g)	Total (µmol/g)	c/Lc

Bambu clay	1483.66	5.37	1620.26	3.69	34.40	31.57	65.97	..92
eta-kaolin	1473.82	9.51	1633.69	3.70	60.92	31.65	92.57	.52
SZY	1454.85	34.37	1650.90	10.85	220.18	93.44	313.62	.42
CZY	1454.86	34.97	1652.91	11.87	224.02	102.20	326.22	.46

4.0 Conclusion

This study discussed the feasibility of developing zeolite Y-type from Bambu clay, as a locally source was investigated, with the aim of producing a material that has comparable characteristics to commercial zeolite Y. The preparation process of the zeolite was carried out in two stages: seed gel and feed gel were synthesized from alumina and silica obtained from local sources.

The result of the XRF analysis indicated that Bambu clay could be kaolinite clay with a Si/Al ratio of approximately 1:8, and the XRD shows the clay contains kaolinite. The XRF and XRD were complimented using the SEM, which shows that the clay possesses psedo-hexagonal and stacking shapes, which represent a kaolinite structure. The clay possesses Lewis and Bronsted acid sites and has a surface area of 159.40 m-2g-1. The synthesized zeolite from Bambu clay shows that the Si/Al ratio of SZY and CZY was 2:40 and 2.62, respectively. From the SEM, the individual particles of SZY and CZY have regular tetrahedral and bulky shapes with average crystallite sizes of 24.77nm and 24.04 nm, respectively. The BET analysis reveals that the surface area of SZY was 549.10 m2g-1 higher than that of the commercial zeolite, CZY (426.20 m2g-1.). The analysis shows that the Lewis and Bronsted acidic sites of SZY are 220.18 and 93.44 µmol/g while the CZY sites are 224.02 and 102.20 µmol/g respectively. The results indicated that SZY had a higher concentration of Lewis acid sites than Bronsted acid sites.

In conclusion, this study demonstrated that the clay possesses kaolinite and, with the Lewis and Bronsted sites, makes Bambu clay a potential source for zeolite synthesis. The SZY possesses similar characteristics to the CZY. The SZY contains a milder acidic site, which favours the cracking of oxygenated hydrocarbons by selecting the organics in bio-oil for catalytic cracking. This study could have a positive impact on the economy of Nigeria in terms of local content.

5.0 References

[1] Abdullahi, T., Harun, Z., Othman, M.H.D., Yusof, K.N., Rahmawati, A., Yunos, M.Z., Lajis, M.A. and Yusof, Y. (2019). Preliminary studies on hydrothermal synthesis of zeolite from Malaysian kaolinite clays. Malaysian Journal of Fundamental and Applied Sciences, **15**(3), 421- 425.

[2] Adeoye, J. B., Omoleye, J. A., Ojewumi, M. E., Babalola, R. (2017). Synthesis of Zeolite Y from Kaolin Using Novel Method of Dealumination. International Journal of Applied Engineering. Vol 12. 5:755-760.

[3] Ajayi, O., A. (2012). Development of large pore zeolite from kaolinite clays. Advances in Chemical Engineering and Science. Vol.10:.4. 226.

[4] Asmaa K. B., Helmy E. H., Ahmed A. M., Ahmed M. A., Manar H. M. (2020). Synthesis and characterization of zeolite-Y from natural clay of Wadi Hagul. Egyptian Journal of Chemistry. 290.

[5] Ayodeji1, A., A., Kofi, H., F., Modupe, O., E., Osayomwanbo, U., J. (2018). Effects of Sodium Hydroxide Concentration on Zeolite Y Synthesized from Elefun Kaolinite Clay in Nigeria. International Journal of Applied Engineering. Vol 13. 3: 1536-1542.

[6] Breck, D., W. (1974). Zeolite molecular sieves: structure, chemistry, and use. New York Wiley. 73011028.

[7] Cadene, A., Durand-Vidal, S., Turq, P.& Brendle, J. (2005). Study of individual Na-motmorillonite particle size, morphology and apparent charge. Journal of Colloid and Interface Science. 285, 719-730.

[8] Khatrin, I., Saragi, I., R., Ekananda, R, Hanna, J., V., Griffith, E., V., Krisnandi, Y., K. (2020). Natural Aluminosilicate-based Y Zeolite for Catalytic Cracking of n-Hexadecane. Makara Journal of Science, 79–85.

[9] Jia, L., Sun, X., Ye, X., Zou, C., Gu, H., Huang, Y., Niu, G. and Zhao, D. (2013). Core–Shell Composites of USY/Mesosilica: Synthesis and Application in Cracking Heavy Molecules with High Liquid Yield. Microporous and Mesoporous Materials. Vol. 176: 16–24.

[10] Kwakye-Awuah B., Von-Kiti E., Buamah R., Nkrumah I., Williams C. (2014). Effect of crystallization time on the hydrothermal synthesis of zeolites from kaolin and bauxite. International Journal on Science Engineering Resources. Vol. 5:734–41.

[11] Madduluri, R., V., Katari, N., K., Peddinti, N., Prathap, C., Burri, D., R., Kamaraju, S., R., R., Jonnalagadda S., B. (2019). Unique Lewis and Bronsted acidic sites texture in the selective production of tetrahydropyran and oxepanefrom1,5-pentanediol and 1,6-hexanediol over sustainable red brick clay catalyst. Heliyon. Vol. 5: 212.

[12] Moises M., P., Da-Silva, C., T., P., Meneguin, J., G., Girotto, E., M., Radovanovic, E. (2013). Synthesis of zeolite NaA from sugarcane bagasse ash. Materials. Vol. 108: 243-246.

[13] Nurudeen S. (2015). Development of zeolite Y and ZSM5 composite catalyst from Kankara kaolin. Department of Chemical Engineering. PhD Zaria: Ahmadu Bello University, Zaria, pp.1-311.

[14] Patel, H. A. (2014). Nanoclay: synthesis, characterisation and application. New Delhi: Journal of Astral.

[15] Salahudeen, N. (2018). Metakaolinization effect on the thermal and physiochemical properties of kankara kaolin. KMUTNB International Journal of Applied Science Technology. Vol. 11, 2: 127-135-

[16] Salahudeen N., Ahmed A., S. (2017). Synthesis of hexagonal zeolite Y from Kankara kaolin using a split technique. Journal of Chemistry. Vol.87:149–56.

[17] Usman, R., A., Kovo, A., S., Abdulkareem., A., S., Garba, M., U. (2022). A facile approach towards Hierarchical Zeolite Y Synthesis from Inexpensive Precursor. Research square. 1

Journal of Engineering, Science, and Technology
ISSN: 2714-2396 | Volume 6, Issue 1

e

DEVELOPMENT OF A SINGLE GRAPHICAL USER INTERFACE PLATFORM-BASED SOLAR PV SYSTEM MODEL FOR EFFECTIVE PV COMPONENT SIZING

Hauwa T. Abdulkarim[1], Christopher L. Sansom[2] and Kumar Patchigolla[3], H. J. A. Almond[4], and M. Karim[5]

[1] Chief Lecturer, Department of Electrical/Electronic Technology, Niger State College of Education, Minna

[2]Professor of CSP & Head of Zero Carbon Theme, University of Derby, Derby, UK

[3]Reader in Carbon Capture, School of Water, Energy and Environment, Cranfield University, UK

[4]Research Fellow, School of Water, Energy and Environment, Cranfield University, UK

[5]Senior Researcher in Solar Energy and Zero Carbon, University of Derby, Derby, UK

Email: [1] talatuabdulkarim@gmail.com, [2] c.sansom@derby.ac.uk,
[3] k.patchigolla@cranfield.ac.uk, [4] h.j.a.almond@cranfield.ac.uk, [5] m.karim@derby.ac.uk

ABSTRACT

The deployment of solar energy system is necessary to meet the energy demands of the rural areas in Nigeria. The investment for the system components is capital intensive and therefore, a techno-economic model which can be used to rapidly design the system is imperative. This paper presents the development of a novel and unique solar PV energy system model (SPVSM) which can be used to accurately size PV system components. It also has energy and economic analysis panels all on a single GUI platform. As a case study, the model was applied to a rural area in Maiduguri, Nigeria. Energy demand of 1.1MWh per day, mean hourly irradiance of 266 W/m2 and mean daily sunshine hours of 7.89 hours which were obtained for a 10-year data of the location were used. The model was applied to accurately size the solar PV components and performed the energy and economic analysis to ascertain its viability. From the energy analysis panel, an annual output of 409.2 MWh was obtained from the system. As for the economic analysis, the capital cost was $2.394 million and considering a system lifespan of 25 years, the Net Present Value (NPV) of the project and the LCOE are $657.96 million and $0.0812/kWh respectively. From the simulation, 2226 number of 300 W module are required. The model developed is quite simple to adapt. The use of solar energy for power supply is highly desirable because it is a source of energy that is inexhaustible, environmentally friendly and economically viable.

Keywords: Solar photovoltaic energy, economic analysis, LCOE, irradiance

INTRODUCTION

The increase in world's population and technological development has undoubtedly led to rapid increase in global energy demand. The most widely used resource for electrical energy generation are the fossil fuels but studies have shown that these resources have negative environmental and health impacts [1]. This has led to the growing interest in the use of renewable energy sources such as solar photovoltaic for power supply.

Nigeria has inadequate supply of energy to both urban and rural areas with about 60% of its population in the rural areas having no access to energy security which is "the uninterrupted availability of energy at an affordable price" [2]. Lack of energy security is one of the major causes of poverty in the rural areas of Nigeria as this is associated to the bad economic and social impacts of either lack of adequate energy, or exorbitant prices that are not competitive

e
or are very unstable [3]. The demand for electricity in Nigeria obviously outweighs the supply, this inadequate supply is further bedevilled with frequent outages and consequently low reliability as a result of inadequate power infrastructure, poor grid network and poor maintenance culture. A large percentage of Nigerians rely on petrol or diesel generators for power supply for both domestic and industrial usage. Nigeria is endowed with verse energy resources such as oil, gas, hydro and solar resource. Figure 1 shows Nigeria's solar radiation map.

The availability of solar energy on the earth depends on the geographical location, time and season. The area under study is indicated on the map by Zone I for Maiduguri. The thick circle close to Maiduguri indicates the location of study which is in the North-Eastern Nigeria. Osueke, Uzendu and Ugbonna [5] studied the variation in solar irradiance in 4 different sites in Nigeria using data acquired from National Aeronautics and Space Administration (NASA) Research and employing SPSS statistical tool and a bar chart. The study concluded among other things that Maiduguri laying at latitude 11.9^{o} and longitude 13.1^{o} seemed to experience highest solar irradiance, which ranges from 5.5 – 6.7 kWh/m^2/day, this translates to 229.2 – 279.2 W/m^2.

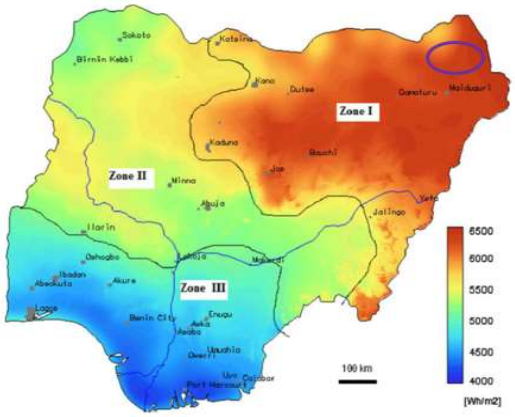

Figure 1: Nigeria's Solar Radiation [4]

The utilization of solar energy to economically meet the ever-increasing energy demand of the world relies on two important aspects: the panel generation factor of the site which is a function of solar irradiance availability and the necessary technology to harness it. To be able to assess the performance of solar energy conversion systems in a location, it is imperative to be aware of the level of solar energy availability at the location. It is clear from Figure 1 that Nigeria is favoured with the availability of solar energy and North-Eastern Nigeria, which is the area under study, is one of the regions most favoured in terms of solar energy availability. Figure 2 shows a typical village in the North-Eastern Nigeria that is not connected to the National grid and has no form of electricity supply and has high solar irradiance which makes solar PV viable.

HOMER (Hybrid Optimisation Model for Electric Renewables) is a micropower computer optimization model that simplifies the task of designing hybrid renewable micro-grids. It has capability for design of off-grid and grid-connected systems. HOMER finds the least cost combination of components that meet electrical and thermal loads. It simulates thousands of system configurations, optimizes for lifecycle cost, and generates results of sensitivity analyses on most inputs [6].

e
SAM (System Advisory Model) is a computer model that calculates and simulates the performance and financial metrics of renewable energy systems such as photovoltaic, concentrating solar power, solar water heating, wind, geothermal, biomass, and conventional power systems. Its advanced simulation options has the capability for parametric, sensitivity and statistical analyses using Monte Carlo simulation and weather variability studies [7]. Past versions of SAM over the years do not have the capability for sizing solar photovoltaic system component until the latest version was released in 2020 with capability to size betteries [8]. Sizing of other components are yet to be included in SAM.

PVsyst is a PC software package for the study, sizing and data analysis of complete PV systems. This software handles grid-connected, stand-alone, pumping and DC-grid (public transportation) PV systems, and includes extensive meteo and PV systems components databases, as well as general solar energy tools. This software is geared to the needs of architects, engineers, researchers. It is also very helpful for educational training. The latest version, PVsyst 7.0, which was released on 25 May 2020 has in its release notes, new features which include economic evaluation such as Levelized Cost of Energy (LCOE), Net Present Value (NPV), multiple loans of multiple types, advanced depreciation configuration economic evaluation now available for Stand-alone and Pumping systems in this latest version.

Figure 1 shows how greatly endowed Nigeria is with solar energy resource and Figure 2 shows how lowly powered the rural communities of Nigeria is. This is to stress the need to invest in solar PV technology for power supply in Nigeria.

The investment for large solar PV power plants is capital intensive, therefore, a solar photovoltaic system model (SPVSM) which can be rapidly used for accurate sizing of the system components for optimized solar PV system for power supply becomes imperative.

Figure 2: Gora Village in North-Eastern Nigeria (Photo by the Researcher during the initial field work)

I. Development of Solar PV System Model on a Single GUI

A. Description of the Model

SPVSM was developed for accurate sizing of solar PV system components (PV array, battery, inverter, and charge controller) and conducting energy and economic analysis of the system. The package has the capability for conducting a sensitivity analysis on the energy and economics of the system considering variation in degradation factor and discount rate. It also

e
gives an economic appraisal such as net present value (NPV) over the expected lifespan of the project. It is built on a single GUI platform but with six executable panels each handling different aspects of component design, energy and economic analysis.

A. Executable Panel 1 - PV array Sizing

Energy demand, E_D is an important parameter required in sizing solar PV array. The peak watt of solar PV module required for any energy demand depends on the Panel Generation Factor (PGF) of the location. Some of the model equations used for the sizing are given in equations 1 and 2. Figure 3 shows the Executable Panel 1. The PGF can be calculated from equation 1.

$$PGF = \frac{Solar\ irradiance\ of\ site \times sunshine\ hours}{Standard\ test\ condition\ irradiance} \quad (1)$$

Designing for 30% higher energy gives equation 2.

$$E_{ARRAY} = E_D \times 1.3 \quad (2)$$

The peak watt W_p, of the solar PV array is given by equation 3:

$$W_p = \frac{E_{ARRAY}}{PGF} \quad (3)$$

For any module rating M_R, the number of modules M_N which is adequate to meet the energy demand is given by equation 4.

$$M_N = \frac{W_p}{M_R} \quad (4)$$

A. Executable Panel 2 - Battery Sizing

Two key parameters that guides the accurate sizing of a battery bank is the energy demand and number of days of autonomy, N_D. Figure 4 shows the executable GUI panel for battery sizing. It should be noted that the energy demand has been declared in the PV module sizing panel.

The battery bank total capacity (Amp.hour) is given by equation 5.

$$Battery\ bank\ capacity = \frac{E_D \times N_D}{V \times DOD} \quad (5)$$

Where V is battery voltage, DOD- depth of discharge and N_D – number of days of autonomy F or a selected battery of amp hour, AH, the total number of batteries required to meet the energy demand is given by equation 6.

$$Number\ of\ batteries = \frac{E_D \times N_D}{V \times DOD \times AH} \quad (6)$$

e

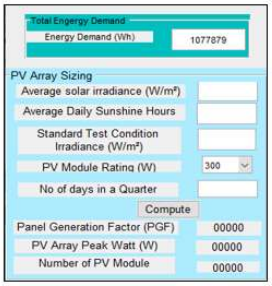

Figure 3: Photovoltaic Module Sizing Executable GUI panel

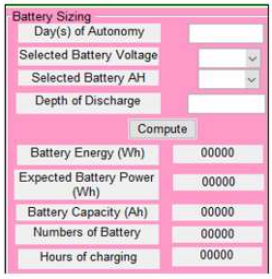

Figure 4: Battery Sizing Executable GUI panel

B. Executable Panel 3 - Inverter Sizing

Usually the inverter is sized 25-30% [9] higher than total wattage demand.. Figure 5 shows the executable GUI panel for inverter sizing. For a load of wattage W_L, the total wattage of inverter required is given by equation 7.

$$W_{T\ INV} = W_L \times 1.3 \qquad (7)$$

the number of inverters to meet the required power for a selected inverter wattage of W_{INV} is given by equation 8.

$$\text{Number of inverters, } N_{INV} = \frac{W_{T\_INV}}{W_{INV}} \qquad (8)$$

C. Executable panel 4 - Charge controller sizing

Figure 6 shows the charge controller sizing GUI executable panel.
The parameters necessary for sizing charge controller are the peak watt of the solar array and the system voltage S_v. Charge controllers are rated in amperes. The total charge controller capacity is given by equation 9.

$$Total\ Charge\ controller\ capacity,\ T_{CC} = \frac{W_P}{S_V} \qquad (9)$$

For any chosen charge controller unit with capacity, CC_C, the total number of such charge controllers that are required is given by equation 10.

$$No\ of\ CC, N_{CC} = \frac{T_{CC}}{CC_C} \qquad (10)$$

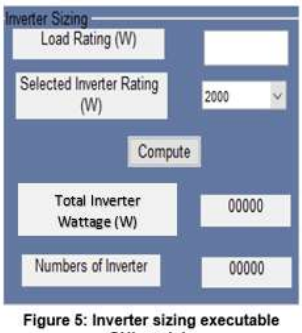

Figure 5: Inverter sizing executable GUI module

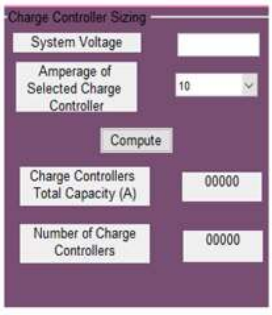

Figure 6: Charge controller sizing executable GUI module

D. Executable panel 5 - Energy analysis

e

The energy from a PV array depends on the peak watt of the array (W_p), conversion efficiency, the daily sunshine hours (SSH) and the average solar irradiance (ASI) of the site. The energy produced by the array per annum can be obtained from equation 11, where STCI is standard test condition irradiance which is 1000 W/m^2. The annual energy over the lifespan of the system is calculated using equation 12. Figure 7 shows the energy analysis panel.

$$E_A = W_P \times \frac{ASI}{STCI} \times SSH \times PV_{Derate} * Efficiency * 365 \quad (11)$$

$$E_A = W_P \times \frac{ASI}{STCI} \times SSH \times DF * Efficiency * 365 * (1 - DEG_A * YR) \quad (12)$$

E. Executable panel 6 - Economic Analysis

The economics of the system was developed bearing in mind the market price of components and some economic assumptions. The economic appraisal methodology employed to assess this proposed PV system is the NPV viz; discount rate of 5%, approach. This gives the present worth of the project by calculating the cash tariff of $0.12, equity of 30% of TPC and loan of 70% of TPC. Where TPC is total project cost. The discount factor, D_F can be obtained from equation 13, where r and YR represents the discount rate and year respectively.

$$D_F = \frac{1}{(1+r)^{YR}} \quad (13)$$

The capital cost can be calculated using equation 14.

$$C_C = PVM_C + INV_C + CC_C + B_C + Ass_C \quad (14)$$

Where PVM_c, INV_c, CC_c, B_c, Ass_c represent costs associated with the PV array, inverters, charge controllers, batteries and other associated costs respectively. Figure 8 shows the economic analysis panel.

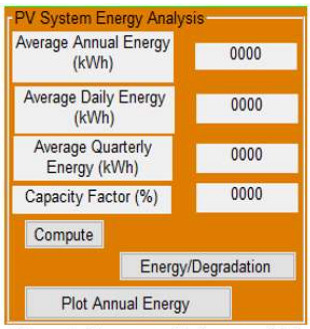

Figure 7: Energy analysis executable GUI panel

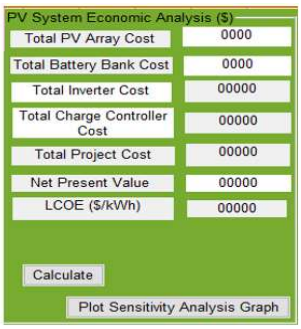

Figure 8: Economic analysis executable GUI panel

RESULTS AND DISCUSSION

After developing the SPVSM GUI, it was subjected to a case study in Maiduguri with energy requirement of about 1.1 MW/day. Figure 9 shows the result of the simulation for each of the six panels on a single GUI platform. Most solar photovoltaic systems which are above 500kW are usually grid-tied but the villages in North-eastern Nigeria being considered in this

e

study are very far from the National grid. In some instances, more than 100 km apart. This distance combined with the frequent power outages makes PV grid-tied system economically and technically unviable for this region. Most software does not handle large solar farms as standalone which is one unique thing about this model (SPVSM).

Solar PV component sizing

Considering the energy demand of 1,077.879 kWh/day and all the other inputs such as irradiance and sunshine hours as it relates to Maiduguri, Figure 9 shows the output of the six panels on a single GUI platform. It displays the accurate sizing of modules, batteries, charge controller and inverter. It also presents the energy and economic analysis. Table 1 shows the sizes of the components.

Table 1: Parameters of solar PV components

	PV Module	Battery	Inverter kW	Charge Controller
Rating per unit	300 W	6V 1200AH	8 kW	80 A
Total No. Reqd.	2225.530 ~ 2226	598.8 ~ 600	20.7	173.86
Total	667.6kW	4.3 MWh	165.6	13909 A

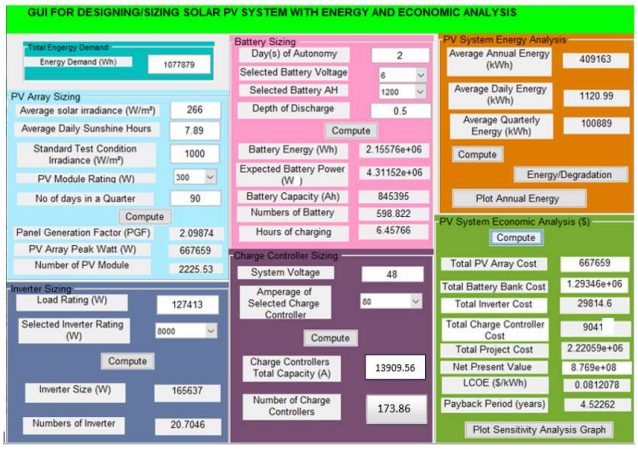

Figure 9: Solar PV System model on a single GUI

F. Energy and Economic Analysis

Figure 10 and Figure11 show the energy and economic analysis of the system. The energy panel shows the average annual, daily and quarterly energy generated by the PV array. The panel also has the capability to present graphical representation of the annual energy generated over the lifespan of the plant taking into account the degradation effect. This is presented in Figure 12. The average annual energy generated by a 667.7 kW power plant is

e
409,163 kWh. Figure 11 shows the cost implications for the designed solar PV system to supply about 1,077.9 kWh of energy per day to a village in the North-eastern Nigeria. The total costs of all major components are presented in Figure 11. The net present value of the plant for estimated lifespan of 25 years is $876.9 million. The levelized cost of energy as shown in the economic panel is $0.0812/kWh. This is in line with the 2019 report of International Renewable Energy Agency. IRENA [10] stated that solar PV projects commissioned in 2018 had a global-weighted-average LCOE of $0.085/kWh. This LCOE according to IRENA [10] is around 13% lower than the equivalent figure for 2017 and that the value has fallen by 77% between 2010 and 2018.

Figure 12 shows the annual energy generated over the lifespan of the plant at varying degradation rates. In the model, a degradation of 1% per annum was assumed, this is in tune with available PV system degradation rates found in literature. Zweibel and Herch (2018), Charaf, *et al.* (2021), Bernard *et al.* (2021) stated that annual degradation rate for solar panel is between 0.5% to 1%. There are two phases, the construction/installation phase and the operation phase. During the construction phase as can be seen in Figure 10, the energy generated is zero obviously. The highest energy output was obtained during the first year of operation as there is least degradation. The energy generated during the fifth year of operation is 402,800 kWh for a degradation of 0.5% and 392,500 kWh for a degradation rate of 1%, this is about a 2.5% drop in energy generated. For the purpose of analysis, PV energy generated was simulated with varying degradation rates. The energy generated during the 25th year of operation for a degradation rate of 1% is 3.099x10^{5} kWh which is 16.6% higher than energy generated for a degradation rate of 1.5% during the same year.

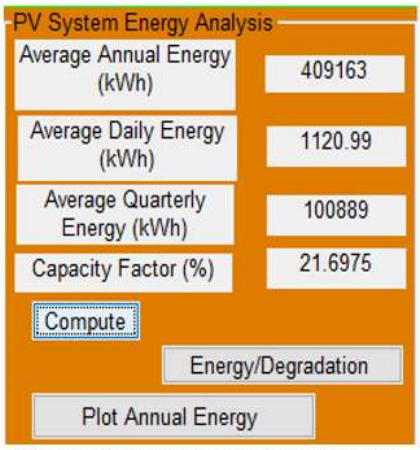

Figure 10: Energy analysis executable GUI panel

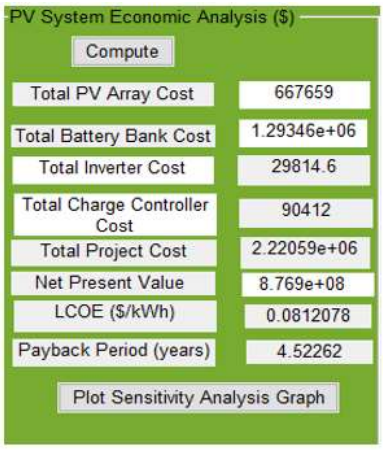

Figure 11: Economic analysis executable GUI panel

Figure 13 shows the graph of annual present value against the year of operation with the sensitivity analysis based on varying discount rates. The sensitivity analysis shows that the annual present value of the system increases from the year of commission to the 17th year of operation and then it begins to decline for discount rate of 5% while decline begins at year 7 of operation for discount rate of 10% During the 1st year of operation, the NPV for a discount rate of 5% is $1.048 million while $0.7285 million for 15% discount factor which gives a 30.5% reduction in NPV. It can be noted there is a downward trend of the annual present value during the construction/installation years, this is because during these years, the cash inflow is obviously zero and therefore the present value which a discounted difference cash inflow and outflow over the lifespan of the plant is negative.

e

The result obtained with the developed model using the case study are in good agreement with those obtained using PVsyst and HOMER.

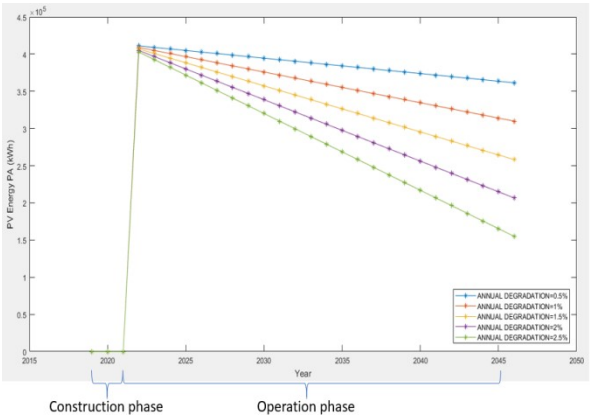

Figure 12: Annual energy over lifespan of project at varying degradation rate

.

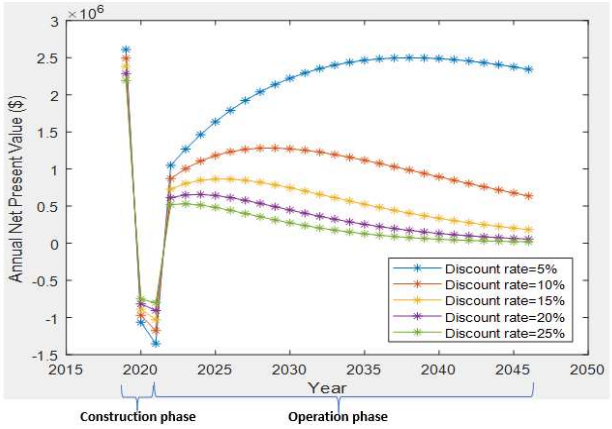

Figure 13: Annual present value over years of operation

CONCLUSION

A solar PV energy system model has been developed. The model which was developed on a single graphical user interface has the capability to accurately size solar PV system components and conduct energy and economic analysis. The model was subjected to a case study in Maiduguri, North-eastern Nigeria. With the knowledge of the required parameters of the site and the energy requirement. The model gave a 2226 number of 300-watt module, 600 number of batteries with rating of 6V and 1200 AH, 21 number of 8000-watt inverter and 174 number of 80 A charge controller. The energy and economic analyses show that the development of solar PV system for power supply in the area under study is economically viable.

Acknowledgement

The authors wish to acknowledge Petroleum Technology Development Fund (PTDF) for the sponsorship, Cranfield University for the facilities and Niger State College of Education, Minna for the study Fellowship.

e

References

[1] Ö. Ayvazoğluyüksel and Ü. B. Filik, "Estimation methods of global solar radiation, cell temperature and solar power forecasting: A review and case study in Eskişehir," *Renew. Sustain. Energy Rev.*, vol. 91, no. May 2017, pp. 639–653, 2018, doi: 10.1016/j.rser.2018.03.084.

[2] IEA, "Global Energy & CO2 Status Report: The latest trends in energy and emissions in 2018," 2019. [Online]. Available: https://www.iea.org/geco/electricity/

[3] IEA, "What is Energy Security," *International Energy Agency*, 2019. https://www.iea.org/topics/energysecurity/whatisenergysecurity/

[4] A. Giwa, A. Alabi, A. Yusuf, and T. Olukan, "A comprehensive review on biomass and solar energy for sustainable energy generation in Nigeria," *Renew. Sustain. Energy Rev.*, vol. 69, pp. 620–641, 2016.

[5] C. Osueke, P. Uzendu, and I. Ogbonna, "Study and Evaluation of Solar Energy Variation in Nigeria," *Int. J. Emerg. Technol. Adv. Eng.*, vol. 3, no. 6, p. 5, 2013.

[6] NREL, "Homer," *Nationaal Renewable Energy Laboratory*, 2014. https://www.nrel.gov/docs/fy04osti/35406.pdf (accessed Sep. 20, 2020).

[7] N. Blair *et al.*, "System Advisor Model, SAM 2014.1.14: General Description," Oak Ridge, 2014. [Online]. Available: www.nrel.gov/publications.

[8] NREL, "System Advisor Model (SAM) Release Notes," 2020. https://nrel.github.io/SAM/doc/releasenotes.html (accessed Sep. 19, 2020).

[9] M. Chandel, G. D. Agrawal, S. Mathur, and A. Mathur, "Techno-economic analysis of solar photovoltaic power plant for garment zone of Jaipur city," *Case Stud. Therm. Eng.*, vol. 2, pp. 1–7, 2014, doi: 10.1016/j.csite.2013.10.002.

[10] IRENA, "RENEWABLE POWER GENERATION COSTS IN 2018," Abu Dhabi, 2019. [Online]. Available: https://www.irena.org/-/media/Files/IRENA/Agency/Publication/2019/May/IRENA_Renewable-Power-Generations-Costs-in-2018.pdf

From the figure, the yield of oil increases steadily as the temperature increases from 60 to 80 ^{O}C with numerical values of 3.73, 4.54, 5.14, 5.66 and 6.69 g corresponding to extraction temperatures of 60, 65, 70, 75 and 80 ^{O}C respectively. As the extraction temperature exceeds 80 ^{O}C the yield began to decline with absolute values of 4.21 and 3.92 g obtained at

extraction temperatures of 85 and 90 ^{e} ^{O}C respectively. At these higher temperatures, some fraction of n-hexane escapes from the condenser thereby reducing the volume of solvent required to extract the oil.

3.2 Effect of Volume of n-Hexane on the
Yield of Oil from African Pear Seed

Fixing the temperature of extraction at 80 ^{O}C and the extraction time of 30 minutes, the volume of n-hexane was varied between 100 to 250 ml with a step change of 50 ml. The results obtained is revealed in figure 4.2

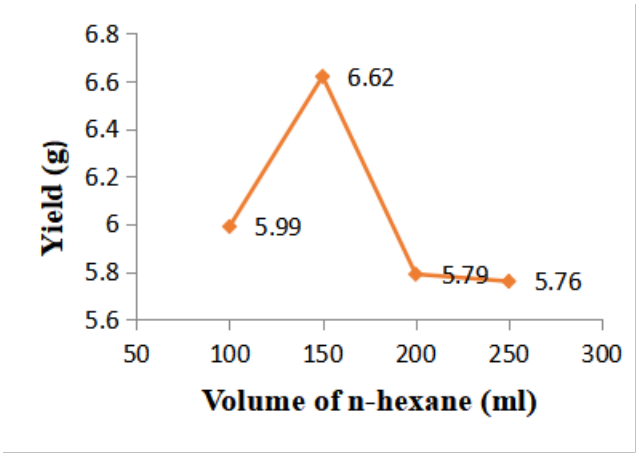

Figure 2: Effect of volume of n-hexane on the extraction of APSO

From the figure, the solvent volume of 150 ml gave the highest yield of 6.62 g APSO and at higher value of solvent volume; the yield of the oil decreases with numerical values of 5.79 and 5.76 g obtained using n-hexane volumes of 200 and 250 ml respectively. At lower volume of 100 ml, the amount of solvent available could not maximize the amount of oil extracted. Higher volume of solvent above 150 ml took longer time before they start boiling thereby reducing the number of reflux under gone by the solvent which subsequently leads to reduction of oil yield.

3.3 Effect of Extraction Time on the Yield
of Oil from African Pear Seed

The effect of extraction time was put into test so as to know the maximum time required to extract oil from the Africa pear seed oil. Figure 4.3 revealed the results of such test and from the result it was evident that the oil yield increases with time and that the maximum time of 60 minutes is required for the extraction of the APSO with a yield of 6.4 g.

e

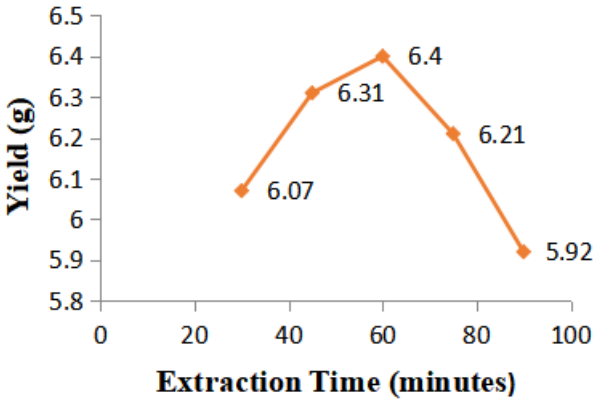

Table 3: Effect of extraction time on the extraction of APSO

At the extraction time of above 60 minutes and temperature of 80 ^{O}C above the boiling point of n-hexane more solvent escapes from the condenser thereby reducing the amount of available solvent to extract the oil. This is the reason why the yield of oil reduces to 6.21 and 5.92 g for the extraction time of 75 and 90 minutes respectively.

3.4 Response Surface Methodology
(RSM) Optimization of Oil Extraction
from Africa Pear Seed

Using the results from the preliminary investigations of the extraction process parameters the three factors investigated and their levels that is lower, midpoint and higher levels is showed in Table 4.1

Table 1: Factors and their levels for Box-Behnken Design

Variable	Symbol	Coded factors level		
		-1	0	+1
Temperature (^{O}C)	A	60	70	80
Volume (ml)	B	100	125	150
Time(min)	C	30	45	60

I Design of Experiment for oil
Extraction from Africa Pear Seed

The inputted coded factors in Table 1 suggested seventeen experimental runs by design expert 13 software using Box-Behnken RSM Design. The From the table, the coded factor levels for the temperature are 60, 70 and 80 ^{O} C for the lower, midpoint and the higher levels while that of the solvent volume and the extraction time are; 100, 125 and 150 ml; 30, 45 and 60 minutes for the lower, midpoint and the higher respectively. Results of these experimental runs carried out as suggested by the software were revealed in Table 2.

Table 2: Experimental yields for Box-Behnken experimental design of APSO extraction

Std	**Run**	**Temp (A) ^{O}C**	**Volume of n-Hex (B) ml**	**Time (C) min**	**Yield (g)**
14	1	70	125	45	4.25

					e
12	2	70	150	60	6.24
13	3	70	125	45	4.24
7	4	60	125	60	5.64
17	5	70	125	45	4.23
15	6	70	125	45	4.44
6	7	80	125	30	5.89
11	8	70	100	60	6.02
1	9	60	100	45	5.29
4	10	80	150	45	6.33
16	11	70	125	45	4.21
9	12	70	100	30	5.01
8	13	80	125	60	5.99
2	14	80	100	45	5.76
10	15	70	150	30	5.12
5	16	60	125	30	3.90
3	17	60	150	45	5.31

From the table, it was observed that the lowest experimental yield was recorded at the run sixteenth (16) with a numerical value of 3.90 g oil yield obtained at temperature of 60 ^{O} C, Solvent volume of 125 ml and extraction time of 30 minutes while the highest yield of 6.33 g was recorded at higher values of the coded factors that is at temperature of 80 ^{O} C, solvent volume of 150 ml and extraction time of 60 minutes. Comparing the results of the lower and the higher yield it is evident that all the coded factors has a positive effect of the yield since all increase in the three, results in an increase in the yield.

When the results of the yields obtained for the experimental design was run with the design expert software, the fit summary Table 3 was generated and the fitted model is a quadratic model

Table 3: Fit summary model for optimization of extraction of APSO

Source	Seq. P-val	Lack of fit P-val	Adjusted R^2	Predicted R^2	Recom
Linear	0.1057	0.0003	0.2190	0.0359	
2F1	0.7462	0.0002	0.0917	-0.3857	
Quadratic	<0.0001	0.1023	0.9691	0.8314	suggested
Cubic	0.1023		0.9868		Aliased

The quadratic model was suggested with a sequential P-value of < 0.0001, lack of fit P-value of 0.1023, adjusted and predicted R^2 of 0.9691 and 0.8314 respectively.

The analysis of variance (ANOVA) was also generated and the result is revealed in Table 4. From the results, the suggested model F- value of 56.76 implies that the model is significant as there is only 0.01 % chance that F-value as large as this will occur due to disturbance. The model terms with P-values less than 0.0500 indicate that those model terms are significant while those with P-values greater than 0.1000 are not significant model terms. In that regard, A, C, AC, A^2, B^2 and C^2 are the significant model terms and on the other hand, B, AB and BC are the insignificant model terms.

e

Table 4: Analysis of variance (ANOVA) for the extraction of APSO

Source	Mean square	F value	P value	Comment
Model	1.17	56.76	<0.0001	Significant
A-Temp	1.83	88.77	<0.0001	
B-Volume	0.1058	5.12	0.0581	
C-Time	1.97	95.38	<0.0001	
AB	0.0756	3.66	0.0973	
AC	0.6724	32.55	0.0007	
BC	0.0030	0.1464	0.7133	
A^2	1.41	68.10	<0.0001	
B^2	2.83	137.23	<0.0001	
C^2	1.07	51.57	0.0002	
Residual	0.0207			
Lack of fit	0.0364	4.13	0.1023	Not Significant
Pure error	0.0088			
Correlation total				

The lack of fit F-value of 4.13 is not significant and therefore suggests that the model well fitted the experimental results. This F-value of 4.13 indicates that there is only 10.23 % chance that this value could occur due to disturbance. The result for the model fit statistics is presented in Table 5.

Table 5: Model Fit statistics for the extraction of APSO

Standard deviation	0.1437
Mean	5.17
Coefficient of variance	2.78
R^2	0.9865
Adjusted R^2	0.9691
Predicted R^2	0.8314
Adequate precision	22.0787

From the result, the predicted R^2 of 0.8314 is in agreement with the adjusted R^2 value of 0.9691 since the difference between the two is less than the maximum allowable threshold value of 0.2. The adequate precision which is a measure of signal to disturbance ratio, suggests that the ratio should not be less than 4. The ratio of 22.079 indicates an adequate signal or precision.

The R^2 value of 0.9865 from this particular research is greater than the value of 0.8454 reported by Adepoju *et al*., (2019) for the same Africa pear seed oil using Box-Behnken RSM Design. When the fit statistics was also compared with that of the work reported by Musa *et al*., (2016) using central composite RSM design for the extraction of Avocado pear seed oil the standard deviation of 0.1437 from this particular research is better than the value of 1.12 reported by Musa *et al*., (2016). The R^2 value of 0.9865 from this research is in closer agreement with 0.9211 reported by Musa *et al*., (2016) while the adjusted R^2 of 0.9691 and

e
the adequate precision of 22.0787 recorded from this work are better than the values of 0.8648 and 13.016 respectively reported by Musa *et al*., (2016).

I The Model equation

The equation suggested by the software in terms of the coded factors is presented as equation (1)

$$\text{Yield (Y)} = +4.27 +0.4788A+0.115B+0.4963C+$$

$$1375AB-4100AC+0.0275BC+0.5780A^2 + 0.8205B^2 + 0.5030C^2 \quad \ldots\ldots\ldots (1)$$

From the ANOVA Table 4, the significant model terms are A, C, AC, A^2, B^2 and C^2. In this regard eliminating the insignificant model terms which are: B, AB and BC, the final model equation for the optimum yield of APSO (*Decryodes edulis*) is given by final equation (2)

$$\text{Yield (Y)} = +4.27 +0.4788A+0.4963C-4100AC+0.5780A^2 + 0.8205B^2 + 0.5030C^2 \quad \ldots (2)$$

The final equation 2 can be used to predict response (yield) of any given level of each factor in the equation and as such, the equation can be extremely useful for identifying the relative impact of the factors by comparing the factor coefficients.

When then the predicted oil yield was plotted against the actual experimental yield, the graph in Figure 4 was obtained. The plot of this nature is usually carried out to see whether the points fall along a straight line in other to come into conclusion that the residuals follow a normal distribution (Umeuzuegbu*, et al*., 2020).

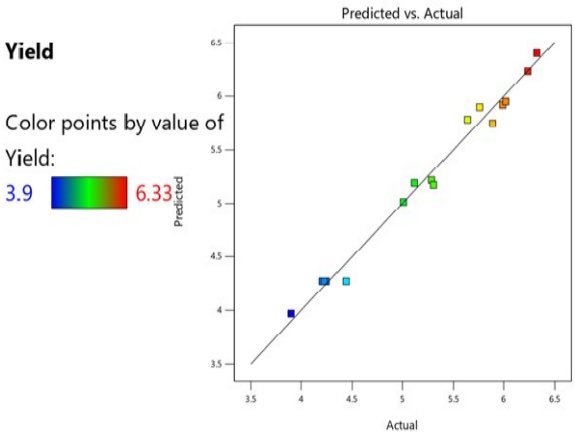

Figure 4: Plot of predicted against actual yield of APSO

The points in Figure 4 were closely distributed along the straight line of the plotted graph and this attest the good relationship between the experimental yields and the predicted yields. The plot also affirms that the selected model adequately predicted the response variables in the experimental values.

II Interactions of process variables

The interactions among the independent variables were represented by 3D response plots that explain the effects of combination of the variables on the yield of oil extracted from the Africa pear seed. Figure 5 shows the interaction between the temperature and the volume of the solvent and both factors has positive effect on the oil yield.

e

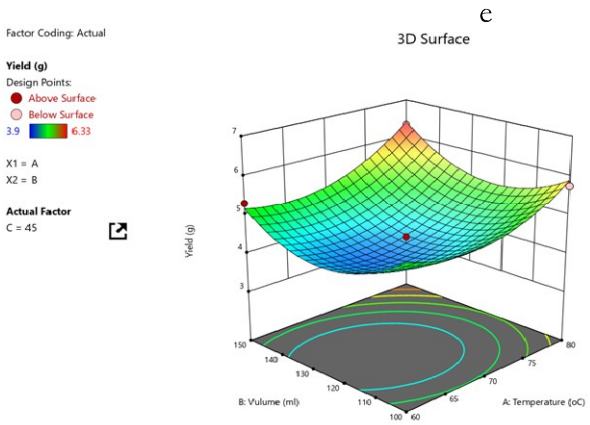

Figure 5: Response surface plot for the interaction between temperature and volume of solvent

The lowest yield recorded by their interaction is 4.44 g oil at a temperature of 70 ^{O} C and solvent volume of 125 ml while the extreme yield of 6.33 g at the highest peak of both the temperature and solvent volume with numerical values of 80 ^{O} C and 150 ml.

Figure 6 shows the interaction between the temperature and time of extraction. The interaction between the temperature and the extraction time follows the same trend of positive impact on the yield when both are increased simultaneously.

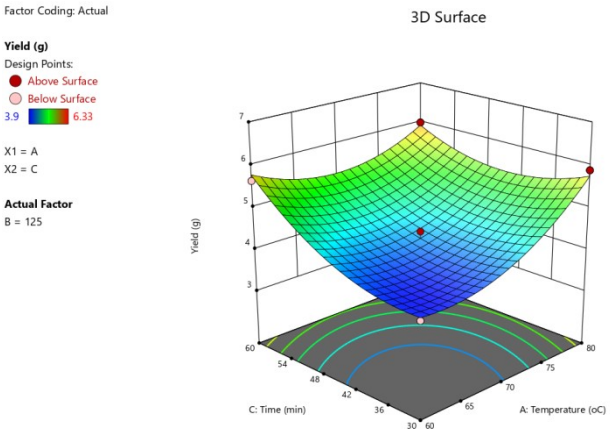

Figure 6: Response surface plot for the interaction between temperature and extraction time

The lowest yield of their interaction at a temperature of 60 ^{O} C and extraction of 30 minutes with a numerical value of 3.90 g oil yield which is the lowest recorded in the research while the highest yield of their interaction is 5.99 g at a temperature of 80 ^{O} C and extraction of 60minutes.

e

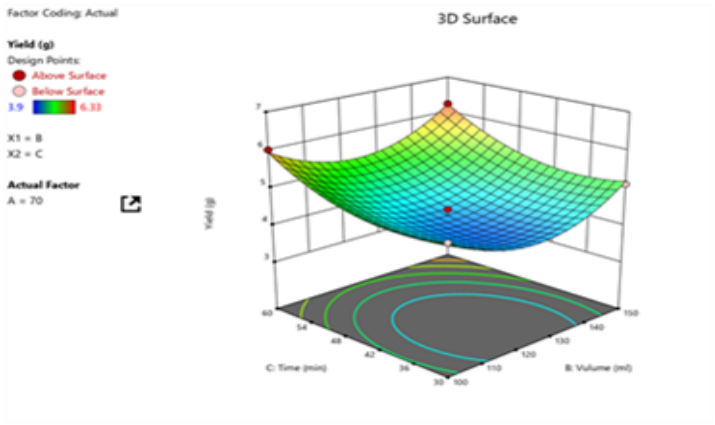

Figure 7: Response surface plot for the interaction between solvent volume and extraction time

The interaction between the extraction time and solvent volume is well described by Figure 7. From the figure, increase in both result in increase in yield of oil. The extraction time of 45 minutes and solvent volume of 125 ml recorded the lowest oil yield of 4.44 g and at the highest level of their interaction at an extraction time of 60 minutes and solvent volume of 150 ml, the highest yield of 6.12 g was obtained.

II Optimum conditions for the extraction of APSO

The optimum conditions suggested for the maximization of the yield of oil from Africa pear seed oil are temperature of 80 ^{O} C, volume of n-hexane of 150 ml and 60 minutes extraction time. The predicted oil yield under these conditions is 7.020 g.

II Validation of APSO Model

For the validation of the model suggested, three set of experiments were carried out at the suggested optimum conditions and the average yield was calculated and compared with the predicted value via standard deviation. The results obtained are presented in Tables 6 and 7.

Table 6: Experimental average yield of APSO at optimum conditions

Run	APSO Yield (g)
1	6.85
2	7.12
3	6.91
Average yield	6.96

From Table 7 the yield of APSO for the three runs are 6.85, 7.12 and 6.91 g while the average yield was calculated to be 6.96 g

Table 7. Standard deviation for optimization of APSO extraction

Parameters	Temp (^{O}C)	Volume ofn-hex	Time (min)	Yield (g)
Optimization Value	80	150	60	7.02
Validation	80	150	60	6.96

e

Value		
	Standard deviation =	**0.04243**

The result of the predicted optimum yield was compared with the experimental average value and the standard deviation was calculated to be 0.04243 as showed in Table 4.8. This low value of the standard deviation further attests the accuracy of the model in predicting the actual experimental results.

3.5 Characterization of Africa Pear Seed Oil (APSO)

I Fourier Transform Infrared Spectrograph (FTIR)

The FTIR analysis was carried out on the APSO in order to determine the various functional groups present in the oil. The FTIR spectrum is presented in Figure 8.

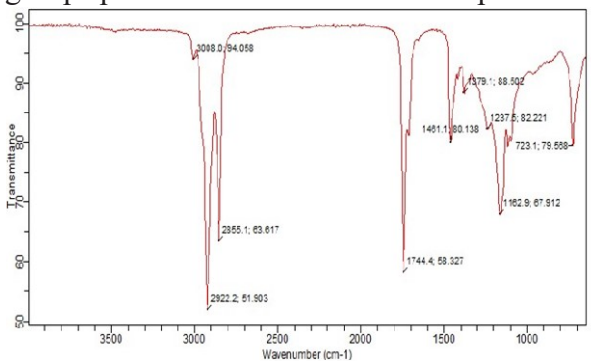

Figure 4.8: FTIR spectrum of Africa pear seed oil (APSO)

From Figure 8, it was depicted that a total of nine (9) absorption bands were identified which means that the oil is a complex organic compound (Asep and Rosid, 2019). The interpretation of the FTIR spectrum depicting the various vibrations and their corresponding functional groups is presented in Table 8.

Table 8: Interpretation of vibrations and functional groups in FTIR spectrum of APSO

S/No	Waveband (cm^{-1})	Vibration	Functional group
1	3008.0	Cis or Trans C-H stretch	Methyl(-CH_3) from an alkene C=C
2	2855.1	Symmetrically C-H stretch	Methyl(-CH_3) froma saturated compound
3	29022.2	Symmetrically C-H stretch	Methylene (-CH_2)From saturated compd
4	1481.1	C=C-C aromatic ring stretch	an Arene 
5	1744.4		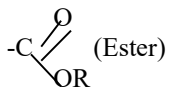 (Ester)
6	1379.1	symmetrically C-H bend	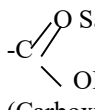 Saturated (Carboxylic acid)

			e
7	1237.5	aryl –O- stretch	Ether C-O-C
8	1162.9	Aromatic aryl –O- stretch	Ether C-O-C
9	723.1	Rocking	$–(CH_2)_n-$ from a saturated fatty acid

From the table considering the single bond region (4000-2500 cm $^{-1}$) of the spectra, three different peaks were identified. The first peak was at 3008.0 cm $^{-1}$ which signify a Cis or Trans C-H stretch vibration from a methyl (CH_3) group from an Aliphatic saturated compound. This is followed by a peak at 2855.1 cm $^{-1}$ indicating a methyl (CH_3) group with a symmetrically C-H stretch vibration while the last peak observed from the single bond region was detected at a wave band of 2922.2 cm^{-1} indicating the presence of a methylene (CH_2) group with a symmetrically C-H stretch vibration.

No peak was detected at the triple bond region (2500-2000 cm $^{-1}$) of the spectra and this signifies that no triple bond compounds are present in the oil complex molecule. Looking at the double bond region of wave band range of 2000-1500 cm $^{-1}$ two peaks were identified one of which is at 1481.1 cm $^{-1}$ signifying the presence of an Aromatic ring with a C=C-C aromatic ring stretch vibration. The remaining peak from this region was observed at a waveband of 1744.4 cm $^{-1}$ signaling the presence of an Ester compound.

The finger print region has the highest number of peaks with a numerical value of four (4) peaks. The first was at a waveband of 1379.1 cm $^{-1}$ indicating the presence of a methyl (CH_3) group with a symmetrically C-H bend vibration from a saturated fatty acid. At a wave band of 1237.5 cm $^{-1}$ an aryl –O- stretch vibration from an ether molecules is dictated while at a lower waveband of 1162.9 cm $^{-1}$ with an aromatic aryl –O- stretch vibration is noticed which is also from an ether compound. The last peak identified from this region was at a waveband of 723.1 cm $^{-1}$ which signifies the presence of a methylene $–(CH_2)_n-$ group with a rocking vibration from a saturated aliphatic compound.

I Fatty Acid Composition of APSO

The fatty acid composition of Africa pear seed oil was determined using Gas Chromatograph and Mass spectrograph (GCMS) and the result of the analysis is revealed in Table 9. Perusing the result of this analysis, it was found that the oil contains both saturated and unsaturated fatty acids with the unsaturated being predominant. Numerically the total unsaturated fatty acids amount to 59.6 % specifically comprising of mono-unsaturated Oleic acid with a composition of 38.86 % and di-unsaturated Linoleic acid with a fraction of 20.74 %.

Table 9: Fatty acids compositions of APSO

Component name	Systematic name	Structural formula	Compo-sition (%)
Palmitic acid	Hexadecanoic acid	$CH_3(CH_2)_{14}COOH$	36.74
Stearic acid	Octadecanoic acid	$CH_3(CH_2)COOH$	3.66
Oleic acid	9-Octadecenoic acid	$C_9H_{18}=C_8H_{15}COOH$	38.86
Linoleic acid	9,12-Octadecadienoic acid	$C_6H_{12}=C_3H_4=C_7H_{14}COOH$	20.74

e

The total composition of saturated fatty acids stands at 40.4 % with palmitic acid having the greater value of 36.74 % while stearic acid is the least with a composition of 3.66 %. The ratio of saturated and unsaturated fatty acids in this particular research is very much comparable with that reported by Ibanga *et al*., (2014) for the same type of oil seed with specific value of 52.38 % saturated fatty acids and 47.62 % unsaturated fatty acids.

Table 10 shows the comparison of the fatty acids composition of APSO obtained from this particular research with those obtained from other researches using same type of seed oil from different location and varieties and also different seed oils.

Table 10: Literature comparison of Fatty acids compositions of APSO

	Fatty acid composition (%)						
Literature	Palmitic	Stearic	Oleic	Linoleic	Eicosenoic	Erusic	Linolenic
This research	36.74	3.66	38.86	20.74	-	-	-
Ogunsuyi & Oyeni (2018)	6.1	7.5	76.0	1.9	-	-	-
Esonye & Onukwali (2018)	10.65	12.54	53.13	-	4.71		
Ibanga *et al*., (2014)	44.31	8.07	42.45	5.17	-	-	-
Abdelghani *et al*., (2021)	11.2	8.5	65.9	-	-	-	-
Purendra, (2018)	1.802	0.669	9.53	14.51	6.976	48.586	11.986

The palmitic acid composition of 36.74 % from this research is comparable with the value of 44.31 % reported by Ibanga *et al*., (2014) for the same type of seed oil (APSO) while this value is far greater than the values of 6.1 % and 10.65 % reported by Ogunsuyi & Oyeni (2018) and Esonye & Onukwali (2018) for the same type of seed oil (APSO). When compared with researches using different seed oils, Abdelghani *et al*., (2021) reported lesser value of palmitic acid composition of 11.2 % from Jatropha Carcus seed oil while Purendra, (2018) reported the smaller palmitic acid composition of 1.802 % for Mustard seed oil.

Looking at the composition of stearic acid of 3.66 %, it can be compared to be of close range with 7.5 %, 8.05 % and 8.5 % reported by Ogunsuyi & Oyeni (2018), Ibanga *et al*., (2014) and Abdelghani *et al*., (2021) respectively since they fall within the same tens values.

The 38.86 % oleic acid from this research is close to the composition of 42.25 % reported by Ibanga *et al*., (2014) for the same seed oil but far less than 76.0 % and 53.13 % reported by Ogunsuyi and Oyeni (2018) and Esonye & Onukwali (2018) respectively for same type of seed oil (APSO). When compared with results of different seed oils, this value is also less than the value of 65.9 % reported by Abdelghani *et al*., (2021) for Jatropha seed oil and far

e
greater than 9.53 % reported by Purendra, (2018) for Mustard seed oil. The total composition of 24.74 % linoneic acid recorded from this research is comparable with 14.51 % reported by Purendra (2018) and greater than 1.9 % and 5.17 % reported by Ogunsuyi and Oyeni (2018) and Ibanga *et al*., (2018) respectively. These similarities and differences in compositions of Africa pear seed oils may be attributed to different species of Africa pear (*Decryodes edulis*) used by different researchers, soil and climatic conditions and the level of maturity of the fruits (Ibanga *et al*., 2018).

I Physicochemical Properties of APSO
The results obtained from the analysis of physicochemical properties of APSO are presented in Table 11

Table 11: Physicochemical properties of APSO

Property	Value	Property	Value
Yield (%)	46.4	Refractive index	1.336
pH	6.7	FFA (%)	4.443
Smoke point (^{O}C)	74	Acid value (mgKOH/g)	8.866
Fire point (^{O}C)	85	Saponification value (mgKOH/g)	213.18
Flash point (^{O}C)	95	Peroxide value (mgKOH/g)	25
Density (Kg/m^3)	0.8419	Viscosity (mPas)	3947.9
Specific gravity	0.8882		

From the Table, the percentage yield of APSO is calculated to be 46.4 % and the pH is 6.7. The density, specific gravity, refractive index, free fatty acid and viscosity are: 0.8419 Kg/m^3, 0.8882, 1.336, 4.443 % and 3947.9 mPas respectively. The Smoke point, Fire point and Flash point of the oil were 74, 85 and 95 ^{O}C respectively while the acid value, saponification value and peroxide value recorded are 8.886, 213.18 and 25 (mgKOH/g) respectively.
The results of the physicochemical properties of APSO obtained from this research were compared with some of the reports from related literatures and such comparison is presented in Table 12

Table 12: Literature comparison of physicochemical properties of APSO

e

Literature	This research	Ibanga *et al.*,(2014) (APPO)	Ogunsuyi & Oyeni (2018) (APSO)	Adepoju *et al*(2019) (APSO)	Chizoo *et al* (2019) (APSO)
Oil yield (%)	46.4	58.23	59.0	17.88	56.40
pH	5.7	-	4.39	-	-
Smoke point (^{O}C)	74	-	170	-	30
Fire point (^{O}C)	85	-	229	-	36
Flash point (^{O}C)	95	-	182	-	148
Density (g/ml)	0.8419	-	-	-	-
Specific gravity	0.8888	0.9000	0.8100	0.9217	0.8885
Refractive index	1.336	-	1.44	-	1.4269
FFA (%)	4.443	3.948	12.33	13.072	3.36
Acid value(mgKOH/g)	8.866	7.854	24.66	27..072	6.57
Saponification value (mgKOH/g)	231.18	227.21	171.10	129.03	249.82
Peroxide value (mgKOH/g)	25	-	45.2	37.60	1.88
Viscosity (Cst)	4.69	-	3.70	-	-

From the Table, the yield of APSO from this research is 46.4 %. This value is less than the values of 58.23, 59.0 and 56.40 % reported by Ibanga *et al*.,(2014), Ogunsuyi & Oyeni (2018) and Chizoo *et al,* (2019) respectively but greater than 17.88 % reported by Adepoju *et al,* (2019). The value obtained falls within the range of 40-64 % yield of Africa pear oil extracted through solvent extraction method reported by Umoti and Okyi (1987). The pH value of 5.7 of acidic range is in agreement with 3.39 reported by Ogunsuyi & Oyeni (2018).The smoke point, fire point and flash points of 74, 85 and 95 ^{O}C are less than the values of 170, 229 and 182 ^{O}C respectively reported by Ogunsuyi & Oyeni (2018). When compared with the report of Chizoo *et al,* (2019), the smoke and fire points from this research are greater than the reported values of 30 and 36 ^{O}C respectively while the value of the flash point is less than 148 ^{O}C reported.

The specific gravity of 0.8888 recorded in this research, is in close agreement with the report of all researchers compared with in Table 12 while the refractive index of 1.336 is comparable and close to 1.44 and 1.42 reported by Ogunsuyi & Oyeni (2018) and Chizoo *et al,* (2019) respectively.
The low value of free fatty acid (FFA) of 4.44 % is close and comparable with the values of 3.948 and 3.36 % reported by Ibanga *et al*.,(2014) and Chizoo *et al,* (2019) respectively and less than the values of 12.33 and 13.072 % reported by Ogunsuyi & Oyeni (2018) and Adepoju *et al,* (2019) respectively.

When the acid value of 8.866 mgKOH/g was compared with the reports from other researchers, it was found that this value is comparable with the values of 7.854 and 6.57 mgKOH/g reported by Ibanga *et al*.,(2014) and Chizoo *et al,* (2019) respectively but less than 24.66 and 27.072 mg KOH/g registered by Ogunsuyi & Oyeni (2018) and Adepoju *et al,* (2019) respectively. In the case of the saponification value, this research identified a value of 231.18 mg KOH/g as against the lower values of 171.10 and 129.03 mg KOH/g reported by Ogunsuyi & Oyeni (2018) and Adepoju *et al,* (2019) respectively but lower than the value of

e
249.82 mg KOH/g registered by Chizoo *et al,* (2019). The value of the saponification value in question is in close agreement with 227.21 mg KOH/g reported by Ibanga *et al*.,(2014). The peroxide value of 25 meq O_2/g recorded from this research is less than 45.20 and 37.60 meq O_2/g recorded by by Ogunsuyi & Oyeni (2018) and Adepoju *et al,* (2019) respectively and greater than the value of 1.88 meq O_2/g registered by Chizoo *et al,* (2019). The viscosity of 4.69 Cst reported from this research is in close agreement with 3.70 Cst reported by Ogunsuyi & Oyeni (2018). These similarities and differences in physicochemical properties may also be due to the use of different varieties of Africa pear seed, different soil type and climatic conditions of the origin of the Africa pear tree (Ibanga *et al*., (2014).

4.0 CONCLUSIONS

The oil extraction from Batati African pear seed was successful optimized with optimum conditions of 80 ^{O}C temperatures, 150 ml volume of n-hexane and 60 minutes extraction time giving rise to an optimum yield of 46.4 %. The results of the characterization of the oil showed that it is comparable with the results reported by other researchers for the same APSO and some different oil seeds. From the results of the percentage yield and characterization of the oil, it can be suggested that it can used as a viable alternative feedstock for biodiesel manufacture.

References

[1] Abdelghani, S., Mourad K. and Omar B. M. (2021). Characterization and fatty acid profile analysis of *Jatropha curcas* L. oil cultivated in the Algerian desert, *Biomass Conversion and Biorefinery*. 1-10 https://doi.org/10.1007/s13399-021-02013-8

[2] Adepoju1, T. F., Esu1, I. O., Olu-Arotiowa, O. A. and Blessed, E. (2019). Oil Extraction from Butter Fruit (*Dacryodes Edulis*) Seeds and its Optimization via Response Surface and Artificial Neural Network, *Nigerian Journal of Technological Development,* 16(2), 56-62

[3] Ajibesin K. K. (2011). *Dacryodes edulis* (G. Don) H J Lam: A Review on Its Medicinal, Phytochemical and Economical Properties. *Res J Medicinal Plant* 5 (1): 32-41. doi: 10.3923/rjmp.2011.32.41

[4] Ayhan, D., Abdullah, B., Waqar, A., and Manzoor, S. (2016). Biodisel production from non-edible plant oils. *Energy exploration and exploitation* 34(2) 290-318

[5] Bull O.S. and George D. M. C (2015). Assessment of Fuel Properties of biodiesel obtained from African pear (*Dacryodeseludis*) Seeds Oil, *International Journal of AdvancedResearch in Science, Engineering and* Technology 2 (10), 894-898 ISSN: 2350-0328

[6] Chizoo E., Okechukwu D. O & Akuzuo U. O. (2019). Effects of Process Variables on the Yield and Viscosity of Methyl Eters derived from *Prunus Amygdalus, Decryodes edulis* and *Chrysophyllum Albidium*, *Sigma J Eng & Nat Sci* 37 (1), 25-40

[7] Djedje B. P. G., Kadji B. R. L., Kone F. M. T., Dabonne S. (2020). Effect of Softening Level on Physico-Chemical Parameters of Safou (*Dacryodes edulis*) Pulp

and Oil Grown in Côte d'Ivoire. *J Appl Biosci. 145 (2): 14852 – 14861. doi:10.35759/JABs.145.2*

[8] Duru M., Amadi C., Ugbogu A., Eze A., Amadi B. (2012). Phytochemical, Vitamin andProximate Composition of *Dacryodes edulis* Fruit at Different Stages of Maturation.*Asian J Plant Sci Res* 2 (4): 437-441.

[9] Helene and Joseph (2022). African pear (Dacryodes edulis) Physical characteristics, Nutritional properties *Agric. conspec. sci.* Vol. 87 No. 1 (1-10)

[10] Ibanga, O. I., Okon, D. E., & Udofo, J. E. (2014). Extracton and characterization of Africa pear oil and it's application in synthesis of surface coatings. *International Journal of Advanced Research in Chemical Science (JARCS) , 1* (4), 14-22.

[11] Kadji B. R. L., Kone F. M. T., Sika A. E., Dabonné S. (2016) Physico- Chemical Properties of Safou (*Dacryodes edulis*) Fruits Grown in Côte d'Ivoire. *J Appl Biosci.* 105: 10103-10110. doi: 10.4314/jab. v105i1.7

[12] Ogunsuyi, H. O., & Oyewo, I. O. (2018). Evaluation of Africa Pear(Dacryodes edulis) seeds oil as a viable feeds stock for biodiesel fuel. *Journal of Emerging Trends in Engineering and Applied Sciences (JETEAS) , 9* (1), 50-56.

[13] Poligui R. N., Mouaragadja I., Haubruge E., Francis F. (2013). La culture du safoutier (*Dacryodes edulis* (G Don) H.J.Lam (Burseraceae)): enjeux et perspectives devalorisation au Gabon (synthès bibliographique). Biotechnol Agron Soc Environ 17 (1): 131-147

[14] Purendra, S. (2018). Physico-chemical investigations of Mustard seed (*Brassica juncea L*), *International Journal of Science Research in Multidisciplinary* Studies, 4(6), 24-27

[15] Todou A., d'Eeckenbrugge G. C., Joly H.I. , Akoa, A., Onana, J-M., Achoundong G. (2013). Climatic Niche of *Dacryodes edulis* (G. Don) H.J. Lam (Burseraceae), a Semi-Domesticated Fruit Tree Native to Central Africa. *J Ecol Natural Environ 5 (9): 231-240*

[16] Umeuzuegbu, J. C., Ezennajiego E. E. and Onukwuli O. D. (2020). Production, Characterization and Optimization of Biodiesel from Gmelina Seed Oil, *World Journal of Innovative Research (WJIR)*, 8(4), 74-86 ISSN: 2454-8236

[17] Umoti, U., Okyi, D. A., (1987).Characteristics and composition of oil and cake of Africanpear. *J. Sci., Food Agr.* 38, 67 – 72.

[18] Youmbi E., Mbeuyo M., Tchinda N. D., Amougou A. (2010). Physico- Chemical Characterisation and Classification of Fruits of *Dacryodes edulis* from the Major Agro-Ecological Zones of Cameroon. *Fruits* 65 (6): 355-365